Journal of Applied Fluid Mechanics, Vol. 18, No. 1, pp. 32-44, 2025.
Available online at www.jafmonline.net, ISSN 1735-3572, EISSN 1735-3645.
https://doi.org/10.47176/jafm.18.1.2547

Numerical Study of the Effect of Corona Discharge on Upward Wake Flow in the Horizontal Axis Wind Turbine Farm

S. Abed Zahmatkesh Pasand[1], S. Karimian Aliabadi[2†], S. K. Ghaemi Osgouie[3] and M. Moshfeghi[4]

[1] *Kish International Campus, University of Tehran, Tehran, Iran*
[2] *Faculty, Tarbiat Modares University, Tehran, Iran*
[3] *Faculty of Engineering and Applied science, university of Regina, Saskatchewan, Canada*
[4] *Sogang University, Seoul, South Korea*

†*Corresponding Author Email: Karimian@modares.ac.ir*

ABSTRACT

Many countries worldwide are showing a growing interest in renewable energy sources, with wind energy being a particularly appealing option for generating mechanical energy. Researchers have explored different techniques for controlling the flow of air, including passive, active, and semi-active methods. In wind farms, the wake flow behind a turbine can be impacted by the flow from other turbines, and to address this issue, plasma-based corona discharge actuators are being considered as one of the most effective methods for reducing fluid flow separation on wind turbine blades. This study employs 2D and 3D numerical simulations to examine the use of corona discharge-based plasma actuators on the leading edge of tandem wind turbines within a wind farm. The study investigates how actuator voltage and frequency affect aerodynamic parameters such as lift, drag coefficients, and efficiency. The study incorporates the use of the Q-criterion to analyze vortex behavior and its interaction with the axial wind turbine body. Fluid flow modeling is conducted using the OPENFOAM software. The findings demonstrate that an escalation in both voltage and frequency of the corona discharge results in a decrease in the Q-criterion, attributed to the heightened ionic flow that diminishes the separation zone. Furthermore, reducing the distance between electrodes also aids in diminishing the Q-criterion values. Additionally, the study reveals that integrating corona plasma at the leading edge of wind turbine blades amplified power generation by more than 3.8%. The corona plasma actuator employed in the study had electrodes spaced 3 mm apart, operated at a voltage of 17 KV, and ran at a frequency of 13 kHz.

Article History

Received February 4, 2024
Revised August 15, 2024
Accepted August 17, 2024
Available online November 6, 2024

Keywords:

Flow control
Active flow control
Axial wind turbine
Corona discharge
Plasma actuator

1. INTRODUCTION

A wind turbine farm comprises multiple wind turbines installed in areas where there are high wind speeds for the purpose of generating clean and renewable energy. These turbines are designed to harness the kinetic energy of the wind and convert it into electrical energy. The blades are one of the critical parts of a wind turbine as they capture the energy of the wind and transform it into rotational motion. Maintaining a stable fluid flow over the surface of the blade is a crucial aspect of wind turbine design and operation. As the wind moves over the surface of the blades, it creates regions of high and low pressure. If there is a significant difference in pressure between these regions, the fluid flow may detach from the blade's surface, leading to a loss of energy and reduced efficiency. Therefore, it is essential to design wind turbine blades that can sustain a stable fluid flow over their surfaces, even in fluctuating wind conditions. This necessitates a thorough knowledge of fluid dynamics and the capacity to optimize the shape and the surface properties of the blades to reduce fluid flow separation (Sanderse et al., 2011; Guerra‐Garcia et al., 2020; Yu et al., 2022; Abed Zahmatkesh Pasand et al., 2023; Belabes et al., 2023; Ramesh Kumar & Selvaraj, 2023a).

Interaction between wake flows is a phenomenon that occurs when wind turbines are sited in a farm. The wake flow is the disturbance of the wind created by the blades of a wind turbine as it moves through the air. This wake flow can have a significant impact on the performance of wind turbines, especially when they are arranged in a

tandem farm. When a wind turbine generates power, it creates a wake behind it that contains lower velocity air compared to the incoming wind. This wake can extend for several rotor diameters downstream and can have a significant impact on the performance of downstream turbines. The wake flow creates turbulence and reduces the incoming wind speed, which can decrease the power output of the downstream turbines. In a tandem wind turbine farm, where multiple turbines are arranged in a line, the wake flow from each turbine can significantly affect the performance of the turbines downstream. The first turbine in the line will create a wake that will impact the performance of the second turbine, and so on. This can result in a reduction in power output for the entire farm. To counteract the negative effects of wake flow, designers use various techniques such as turbine spacing, orientation, and blade design. Proper spacing between turbines can reduce the wake flow impact on downstream turbines, while blade design can help reduce turbulence and increase power output. Additionally, proper turbine orientation can help to minimize wake flow impact. In conclusion, wake flow is a significant factor that affects the performance of wind turbines, especially in a tandem wind turbine farm. Proper design and placement of turbines can help mitigate the negative effects of wake flow and improve the overall efficiency of the farm. As the demand for renewable energy continues to grow, it is essential to optimize wind turbine technology to maximize power output and reduce the cost of wind energy production (Sanderse et al., 2011; Guerra - Garcia et al., 2020; Yu et al., 2022; Abed Zahmatkesh Pasand et al., 2023; Belabes et al., 2023).

In the last two decades, researchers are trying to improve engineering systems by using different active flow control techniques (Shams Taleghani et al., 2012; Sheikholeslam Noori et al., 2020a). The advancement of fluid engineering requirements has led to the development of active flow control actuators such as plasma actuators (Shams Taleghani et al., 2012), modulated pulsed jet vortex generators (Abdolahipour et al., 2021, 2022), and surface acoustic waves for droplet motion and water removal from a solid surface (Sheikholeslam Noori et al., 2020b, c, 2021; Taeibi et al., 2022). To enhance the performance of wind turbines, researchers have explored various techniques, such as active flow control over the airfoil. Mohammadi et. al. (2014) used the dielectric barrier discharge to increase stall angle of a NACA0012 airfoil. This method has been utilized in various studies, including De Giorgi et. al. (2021), Benmoussa and Páscoa (2023), Salmasi et al. (2013), Mirzaei et al. (2012), and Yang & Zhang (2023). The corona discharge plasma actuator is one of the common types of plasma actuators that have been used by researchers to flow control applications. This method has been utilized in various industrial settings, such as surface treatment, chemical synthesis, and air purification. In recent times, researchers have been exploring the use of corona discharge in wind turbine technology to enhance the aerodynamic performance of turbine blades.

The leading edge of wind turbine blades is susceptible to fluid flow separation, which can decrease the blade's aerodynamic efficiency and lead to higher maintenance costs and reduced power output. To address this, researchers have suggested the use of corona discharge to alter the surface properties of the leading edge, thereby reducing the separation zone and improving the blade's performance (Gulski et al., 2021). This approach involves using corona discharge to create a plasma layer around the leading edge of the blade. The plasma layer changes the surface properties of the blade, making it more hydrophilic, and promoting the attachment of fluid flow to the surface. Consequently, the separation zone is reduced, and the blade's aerodynamic efficiency is improved. Several studies have demonstrated encouraging outcomes when utilizing corona discharge on wind turbine blades' leading edge. Although the use of corona discharge in wind turbine technology is still in its early stages, it shows immense potential to enhance the performance of wind turbines (Kaviani & Moshfeghi, 2023). However, certain challenges need to be addressed, such as developing durable and cost-effective corona discharge systems that can withstand the harsh environmental conditions of wind turbines. Nevertheless, this technology has the potential to significantly contribute to the growth of renewable energy and reduce our reliance on fossil fuels (Wang et al., 2018; Qu et al., 2019, 2021).

Electric discharge actuators are composed of two electrodes placed asymmetrically on either side of a dielectric material. These electrodes are subjected to high voltage, which creates plasma discharge, inducing a volumetric force over the leading edge of the blade. This force corrects the velocity profile, preventing the boundary layer from expanding outward, thereby controlling the flow. Roth (2003) conducted a fundamental study in the field of plasma actuator for flow control, while Enloe et al. (2004) and Thomas et al. (2009) analyzed the effects of frequency, voltage, and dielectric material on the induced driving force. A comprehensive experimental study of the effects of the geometrical and electrical parameters of the plasma actuator under unsteady excitation conditions on the characteristics of the induced unsteady velocity such as instantaneous velocity, turbulent intensity, and vortex shedding frequency has been carried out by Shams Taleghani et al. (2018).

Durscher & Roy (2012) studied the effect of the induced velocity profile downstream of the actuator, and their studies formed the foundation for introducing plasma discharge-based chemical models and algebraic models (Benard & Moreau, 2014). The algebraic models proposed by Suzen and Huang (2005), which consider the Maxwell equations to simulate the electric potential field and charge density distribution, attracted significant interest from researchers. However, this model requires recalibration with changes in operational and geometric conditions, as well as determining coefficients by conducting experimental tests. Ibrahim and Skote (2011) proposed new boundary conditions for the charge density distribution and dielectric surface length, and their results showed high accuracy in problem-solving approaches. The study conducted by Zheng et. al. (2013) focused on establishing plasma corona discharge over a surface to investigate the significance of plasma on curved surfaces like blades. Herein, their findings have been used to validate the application of plasma corona discharge.

Another study by Abdollahzadeh et. al. (2014a) analyzed the distribution of the charge density using a correction factor. They studied the impact of the distribution of the charge density on the agreement of velocity profile with experimental results.

Omidi and Mazaheri (2017) also corrected the charge density distribution and dielectric surface length. Several researchers have investigated the numerical effects of plasma actuators on the flow field over or inside various geometries, using the model proposed by Suzen and Huang (2005) as a basis for their research. Abdollahzadeh et. al. (2014b) studied the effect of a plasma actuator on the aerodynamic characteristics of a NACA 0021 airfoil with a 23-degree angle of attack, and their results showed a reduction in the separation region and improved aerodynamic characteristics. In another study, they investigated the effect of applying a steady or time-modulated plasma actuator on the separation and reattachment regions, pressure coefficient distribution, and aerodynamic characteristics of a NACA 0012 airfoil, which had similar results to their previous work (Abdollahzadeh et al., 2018). They suggested that the performance of plasma actuators may be worse in a modulated state than in a steady state, depending on the excitation mode and that the operating conditions of the steady state must be carefully selected and analyzed.

Ebrahimi and Hajipour (2018) analyzed the numerical effect of two plasma actuators installed at the leading edge on the suction side and the trailing edge on the pressure side of a NACA 4415 airfoil. They investigated the simultaneous and separate effects of each actuator on the boundary layer instability and separated flow behavior. Ebrahimi et al. (2018) studied the effect of these actuators on the pressure distribution around a NACA0015 airfoil under complete stall conditions, subjected to a flow regime with a Reynolds number of 300,000 and an angle of attack of 14 °. Their results showed that the simultaneous application of the two actuators had a desirable effect on reducing stall.

Maas (2023) compared the Large Eddy Simulation (LES) turbulence model of offshore wind farms with two analytical wake models to identify any discrepancies. The results revealed novel phenomena, such as crosswise divergence and convergence, in a finite-sized wind farm with a multi-gigawatt capacity. The comparison of the wake models with the large-eddy simulation showed significant deviations of up to 40% in the expected power output of the wind farm. Sinner et al. (2023) utilized an innovative technique to evaluate the wind field upstream of a wind turbine. They examined the controller's performance sensitivity to the assumed propagation delay by analyzing a range of wind input sequences. Their research indicated that the preview-enabled controller outperforms the feedback-only scenario over a broad range of assumed propagation delays, demonstrating a degree of resilience to the time alignment of incoming disturbances.

The objective of the study is to reduce wake flow behind wind turbines. In wind turbine farms, wake flow can have a significant impact on the last column of wind turbines. This study utilized a type of plasma actuator known as a corona discharge actuator to address this issue. Considering the voltage on the rough surface of the airfoil, an electric field is formed around the airfoil, which causes the induction of ionic wind or electric wind in the vicinity of the airfoil. This electric wind can influence the boundary layer around the airfoil and delay the separation of the fluid. The plasma generated in the vicinity of the plasma actuator produces a body force that causes the surrounding fluid to move, resulting in the formation of a fluid jet that improves the boundary layer flow profile and delays flow separation. The studies so far have been limited to specific frequency, voltage, and angle of attack conditions, and a general study on the effect of this phenomenon in wind turbine farms with the interaction between wind turbines has not been conducted yet. Therefore, this article attempts to address this gap in the previous work. This research can be a suitable basis for cost-saving calculations to approach industrial applications.

2. GOVERNING EQUATION

In this study, first the formulation related to the creation of electrohydrodynamic wind (ionic wind) by electrodes is presented. Then, by applying the equations of relative humidity and considering the heat equations, the direct relationship between the plasma corona discharge phenomenon and two environmental parameters of relative humidity and temperature has been taken into account. Maxwell's equations have been used to obtain the electric field. Due to the absence of magnetic induction and magnetic field, the resulting equations for electric potential and charge density will be in the form of equations 1 and 2 (Suzen & Huang, 2005; Ibrahim & Skote, 2011).

$$\nabla.(\varepsilon_r \nabla\phi) = 0 \tag{1}$$

$$\nabla.(\varepsilon_r \nabla\rho_c) = \frac{\rho_c}{\lambda_D^2} \tag{2}$$

In these equations, ϕ is the electric potential, λ_D^2 is the square of the Debye length, ρ_c is the charge density, and ε_r is the electric permittivity. Dimensionless boundary conditions are introduced in equations 3 and 4, and constant values are applied to the electrodes and the spreading surfaces. After calculating the dimensionless electric potential and charge density distribution, the obtained values are multiplied by the dimensionless parameters (Suzen & Huang, 2005; Ibrahim & Skote, 2011).

$$\phi^* = \frac{\phi}{\phi_{max} f(t)} \tag{3}$$

$$\rho_c{}^* = \frac{\rho_c}{\rho_c{}^{max} f(t)} \tag{4}$$

In these equations, ϕ_{max} is the maximum electric potential and $\rho_c{}^{max}$ is the maximum charge density. f(t) is the waveform of the applied alternating voltage to the electrodes. By solving the Laplace equation (equation 1) for the distribution of electric potential and the Poisson equation (equation 2) for the charge density, and considering that the electric field is equal to the gradient

of the electric potential, the volumetric force applied by the actuator can be obtained (Suzen & Huang, 2005; Ibrahim & Skote, 2011).

$$E = -\nabla\phi \tag{5}$$

$$F_b = \rho_c E \tag{6}$$

In this equation, E is the electric field and F_b is the volumetric force. The equations above contain unknowns, and their calculation methods will be presented later. Equation 7, which is based on the latest corrections made to this parameter, is used to determine the Debye length (Suzen & Huang, 2005; Ibrahim & Skote, 2011).

$$\lambda_d = 0.2\ (0.5611 Arctan(-170.3(f)^{-5.124}) + 1.768) \times (0.3 \times 10^{-3} V_{app} - 7.42 \times 10^{-4}) \tag{7}$$

In equation 7, f is the frequency of the sinusoidal wave, measured in kilohertz, and V_{app} is the peak voltage in kilovolts. Additionally, to calculate the plasma spreading length, it is necessary to solve the system of algebraic equations, equation 8, using the Newton-Raphson method (Suzen & Huang, 2005; Ibrahim & Skote, 2011).

$$a_1^2 l_p^5 + 2a_1 a_2 l_p^4 + a_2^2 l_p^3 = a_3^2 \tag{8a}$$

$$a_1 = 16000 c_{g0} \tag{8b}$$

$$a_2 = 16000 c_{d0} I_e \tag{8c}$$

$$a_3 = \sqrt{\rho} f c_{g0} c_{d0} I_e (V_{app} - V_{bd})^2 \tag{8d}$$

All of the above equations are included in the developed solver in the *OPENFOAM* software. The iterative Newton-Raphson method for calculating the plasma spreading length is implemented within the basic solver in *OPENFOAM*, and it is sufficient to obtain the plasma spreading length by invoking the appropriate boundary conditions. In equation 8, ρ is the fluid density, I_p is the plasma spreading length, I_e is the hidden electrode width, and V_{bd} is the breakdown voltage. Considering that the visible and hidden electrodes are considered as a series circuit, the capacitance of each capacitor can be expressed using equations 9a and 9b (Suzen & Huang, 2005; Ibrahim & Skote, 2011).

$$c_{g0} = \frac{2\pi\varepsilon_0}{ln\left(\frac{0.5t_e + \lambda_d}{0.5t_e}\right)} \tag{9a}$$

$$c_{d0} = \frac{2\pi\varepsilon_d}{ln\left(\frac{0.5t_e + 2t_d}{0.5t_e}\right)}, \quad \varepsilon_d = \varepsilon_{rd}\varepsilon_0 \tag{9b}$$

The permittivity of free air is ε_0, and the permittivity of the dielectric material is ε_{rd}. t_d is the thickness of the dielectric, and t_e is the thickness of the electrodes. Equation 10 is used to calculate the maximum charge density (Suzen & Huang, 2005; Ibrahim & Skote, 2011).

$$\rho_c^{max} = \frac{Thrust}{\lambda_d (V_{app} - V_{bd}) f_{corr}}$$

$$f_{corr} = 0.5\sqrt{2\pi}\frac{a}{l_p^{corr}}\left[\left(\frac{1}{2}\frac{b\sqrt{2}}{a}\right) + erf\left(\frac{1}{2}\frac{\sqrt{2}(l_p^{corr} - b)}{a}\right)\right] \tag{10}$$

The coefficients a and b in the correction factor are 0.32 and 0.17, respectively, multiplied by the plasma spreading length, and the induced thrust due to the actuator operation is obtained using equation 11 (Suzen & Huang, 2005; Ibrahim & Skote, 2011).

$$Thrust = [4\rho(2fC_{eq}(V_{app} - V_{bd})^2)^2]^{\frac{1}{3}} \tag{11}$$

After calculating the volumetric force applied by the actuator, it is necessary to solve the continuity and momentum equations within the computational domain. The incompressible and steady-state form of the Navier-Stokes equations is expressed in equation 12. (Suzen & Huang, 2005; Ibrahim & Skote, 2011; Nazari et al., 2021, 2023).

$$(\vec{V}.\nabla)\vec{V} = -\frac{1}{\rho}\nabla P + \nu\nabla^2\vec{V} + \vec{f_b} \tag{12a}$$

$$\nabla\vec{V} = 0 \tag{12b}$$

$$c_p \frac{\partial \vec{V}T}{\partial x_j} = -\frac{1}{\rho}\nabla.(k\nabla T) + \frac{1}{2}\tau:(\nabla\vec{V_j} + \nabla\overrightarrow{V^T_j}) \tag{12c}$$

For all the simulations conducted in this study, the researchers used the k-ε turbulent model, which is a commonly accepted standard. Previous research has demonstrated that this model is dependable when it comes to simulating wind flow in wind turbine farms. Additionally, it has a relatively low computational cost, as per the suggestions of researchers (El Kasmi & Masson, 2008).

3. METHODOLOGY

For this study, a three-dimensional model of a 2 MW wind turbine with 24 tandem turbines was developed. The model represents a zone with six standing locations divided into four rows. All turbines are assumed to have the same dimensions and are represented as blocks with a height of 75 (m) (Table 1). A highly refined unstructured mesh with near-wall refinement is used, with a maximum mesh size of ~20 mm and a minimum cell size of ~1.3 mm. To ensure similarity between the computational mesh of different turbines, only one mesh is generated near the turbine, and all turbines have the same mesh refinement. A Multiple Reference Frame (MRF) zone with 6 DOF was used to account for the rotation zone of the turbine blades. Salome software (version 6) and SnappyHexMesh utility were used to generate and discretize the wind turbine. The simulation was conducted in 2D to better understand the effects of plasma corona discharge on reducing the separation zone behind the blades. Boundary conditions and dimensionless equations were applied to the boundaries and computational domain. The convergence criterion for the problem was taken as the residual values of flow characteristics 10^{-7}.

The geometrical model was complex, and an unstructured grid was used, which was adapted to various geometric structures. The mesh-independent test results were satisfactory, and no additional refinement of the base mesh was necessary. The boundary conditions applied to the computational domain in Fig. 2 included a dimensionless potential of one on the visible electrode

Table 1 Dimensions of computational domain for 2D and 3D simulations

Section	Name	Dimensions
Plasma Corona dimensions (2D and 3D simulation)	Anode	7 mm
	Cathode	4 mm
	Distance between anode and cathode	3 mm
Airfoil wind turbine dimensions (2D simulation, Fig. 1d).	Length of a chord	250 mm
	Maximum thickness of airfoil	45 mm
	Location of maximum thickness	35% of the chord length from the leading edge
Wind turbine farm dimensions (3D simulation, Fig. 1a)	Length of farm domain (L)	240 m
	Width of farm domain (W)	120 m
	Height of farm domain (H)	90 m
	Minimum distance between wind turbines	30 m
	Maximum distance between wind turbines	40 m
	Height of wind turbine	75 m

Table 2 Dependency study of the computational domain size with a total of 5×10^6 meshes

Domains	Value of dimensions	C_D	C_L
Case 1	farm domain Length (L) of 220 m farm domain Width (W) of 100 m	0.512	0.181
Case 2	farm domain Length (L) of 240 m farm domain Width (W) of 120 m	0.540	0.200
Case 3	farm domain Length (L) of 280 m farm domain Width (W) of 160 m	0.539	0.200

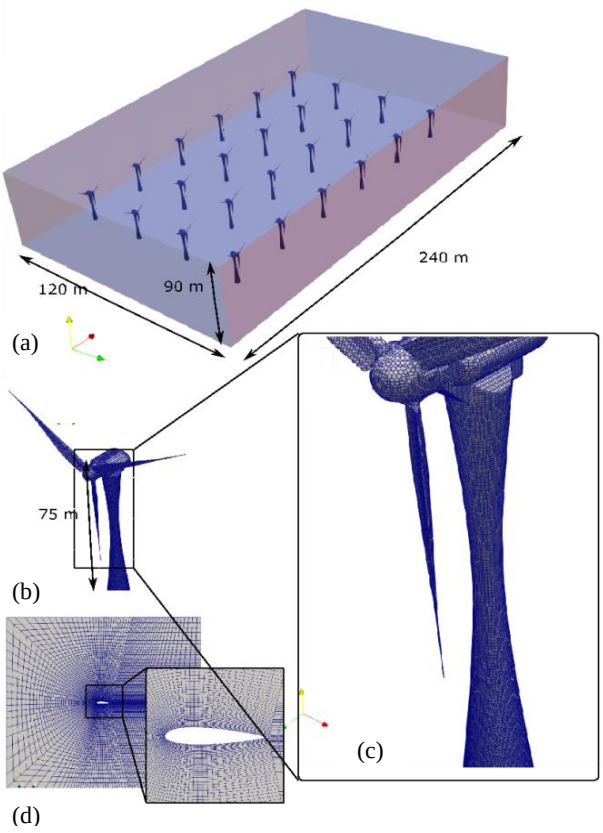

Fig. 1 Illustration of (a) wind turbine farm dimensions, (b) high resolution of unstructured meshes over the wind turbine, (c) height of wind turbine (d) the computation mesh used in the CFD simulations and structured mesh in 2D section of simulations

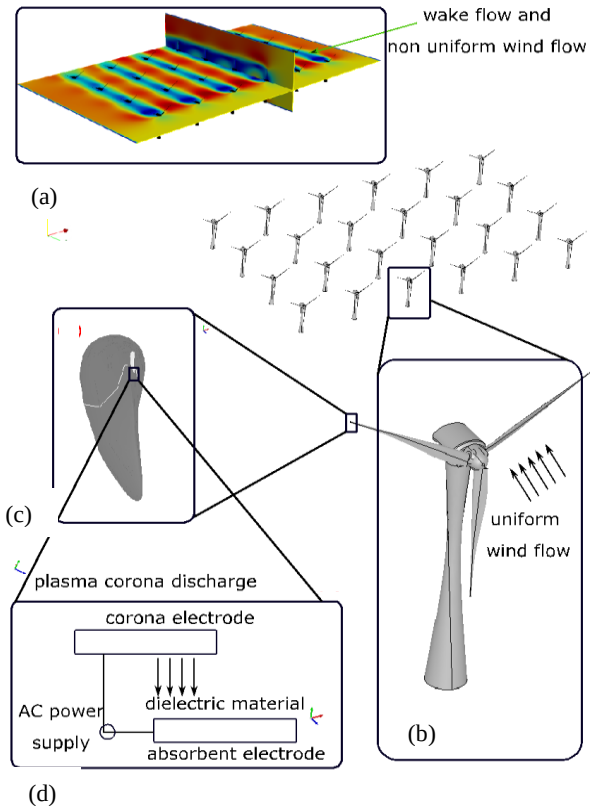

Fig. 2 Illustration of (a) velocity contour of wind turbine farm and uniform and non-uniform Q criteria distributions, (b) wind flow direction near the blades, (c) cross section view of wind turbine blade and leading edge (d) the applied plasma corona discharge near the edge

Table 3 Boundary conditions for 2D and 3D sections of present numerical work, Initially, a 2D simulation was conducted solely to validate the effects of plasma corona discharge over a single blade. Once the configuration was validated, it was then applied to a 3D domain

Section	Name of boundary	Boundary condition
Plasma Corona dimensions (2D and 3D simulation)	Corona electrode	Constant velocity, pressure flux and equations of $\phi^* = \frac{\phi}{\phi_{max} f(t)}$ and $\rho_c{}^* = \frac{\rho_c}{\rho_c{}^{max} f(t)}$
	Absorbing electrode	Constant velocity, pressure flux and equations of $\phi^* = \frac{\phi}{\phi_{max} f(t)}$ and $\rho_c{}^* = \frac{\rho_c}{\rho_c{}^{max} f(t)}$
	Debye length (λ_d)	$\lambda_d = 0.2(0.5611 tan^{-1}(-170.3(f)^{-5.124}) + 1.768) \times (0.3 \times 10^{-3} V_{app} - 7.42 \times 10^{-4})$
	Permittivity (ε_r) and density (ρ_c)	$\nabla.(\varepsilon_r \nabla \rho_c) = \frac{\rho_c}{\lambda_D^2}$
Airfoil wind turbine dimensions (2D simulation, figure 1d)	Inlet	Constant velocity, pressure gradient equals zero
	Outlet	Atmospheric pressure, zero velocity gradient
	Airfoil wall	No slip velocity
Wind turbine farm dimensions (3D simulation, figure 1a)	Inlet of farm	Constant velocity of 15 kilometers per hour, pressure gradient equals zero
	Outlet of farm	Atmospheric pressure, zero velocity gradient
	Wind turbine walls	No slip velocity
	MRF	The circular domain surrounding the blades has the same dimensions as the blade diameters. The blades are capable of six degrees of freedom movement, and the pressure gradient is set to zero. With these six degrees of freedom movement, the blades are free to rotate due to the applied force from the air and their design shape, rather than being forced.
	Far-fields	free-stream velocity, pressure far-field

surface and zero on the hidden electrode surface. The dimensionless charge density was zero at the surrounding boundaries, and the electric potential gradient was zero. At the common boundary of the dielectric and air, the condition of zero dimensionless charge density gradient was imposed, and the distribution of charge concentration on the plasma expansion surface was assumed to be semi-Gaussian. Inlet velocity boundary conditions were used at the surrounding boundaries of the airfoil in the front, top, and bottom, and outlet pressure conditions were used at the outlet boundary at the back of the airfoil. A wall boundary condition was used on the surface of the airfoil. The high-order method was used for the turbulent kinetic energy, charge concentration, and electric potential to discretize the momentum equation.

In the current study, we opted for the dimensions specified in Table 1 for the 2D and 3D computational domains. To guarantee that the boundaries do not impact the numerical solution, we conducted a study on the dependency of the computational domain size. Table 2 presents the results of this study for a 3D wind farm, focusing on a wind turbine positioned along the central horizontal axis. The findings indicate that the dimensions of case 2 (as outlined in Table 1) are appropriate, as increasing the computational domain size does not lead to significant changes in the results.

The effect of a plasma discharge actuator on controlling flow separation around a critical section of a wind turbine blade at one angle of attack was numerically investigated. This section, located at 25% of the blade length from the blade tip, experiences the highest aerodynamic loads and is important for further studies. The numerical simulation was carried out using *OPENFOAM* software, and a comparison was made between the results obtained at angle of attack of 20 °. After ensuring the accuracy of the simulation, the effect of operational conditions such as voltage and frequency of the actuator on aerodynamic efficiency, size of the separation region, boundary layer separation point, suction and pressure coefficients of the airfoil, and flow turbulence intensity was studied at angle of attack of 20°. The computational domain was created at a distance of 40 times the chord length of the airfoil from the back and extended to 25 and 15 times its length from the sides to ensure that the boundaries did not affect the numerical solution. Table 3 displays all the boundary conditions used in the current numerical study. A two-dimensional structured computational grid was created around the airfoil, and a structured grid was created for the space outside the airfoil surface and around the electrodes. The plasma actuator equations were solved independently of the fluid flow equations, and after solving and converging the results of the plasma actuator equations (charge density and electric potential), the solution of the flow field equations was started. To create an ionic wind, the *EHD* solver in *OPENFOAM* was combined with the BPF (*BoussinesqPimpleFoam*) solver. The numerical investigation focused on a critical section of the wind turbine blade that experiences high aerodynamic loads, located at 25% of the blade length from the tip. The effect of using a plasma discharge actuator on controlling flow separation around this airfoil was studied at one angle of attack using *OPENFOAM* software. After ensuring the accuracy of the numerical simulation, the impact of operational conditions such as voltage and frequency of

the actuator on aerodynamic efficiency, size of the separation region, boundary layer separation point, suction and pressure coefficients of the airfoil, and flow turbulence intensity was studied at angle of attack of 20°. The computational domain was created at a distance of 40 times the chord length of the airfoil from the back, and a structured grid was developed for the space outside the airfoil surface and around the electrodes. The plasma actuator equations were solved independently of the fluid flow equations, and the results were converged before solving the fluid flow equations. This combination allowed for a comprehensive and accurate numerical investigation of the effect of plasma discharge actuator on controlling flow separation in wind turbine blades.

3.1 Q Criteria

The Q criteria is a technique utilized in fluid mechanics to detect vortices in fluid flow by determining their strength and location. Vortices refer to regions of swirling flow characterized by the rotation of fluid particles around an axis, and they are prevalent in various fluid flow applications, including aerodynamics, oceanography, and industrial processes. The Q criteria involves analyzing the second invariant of the velocity gradient tensor to identify vortices mathematically. This mathematical method operates on the premise that vortices have high values of the second invariant, whereas non-vortex regions have low values of the second invariant. The Q criteria can be expressed mathematically as (Zhang et al. 2019):

$$Q = \lambda 2 - \lambda 3 \tag{13}$$

The Q criteria is a scalar field that is calculated using the second and third eigenvalues of the velocity gradient tensor ($\lambda 2$ and $\lambda 3$, respectively) and provides a quantitative measure of the strength and location of vortices in the fluid flow field. This method is useful for visualizing and analyzing vortex behavior in fluid flow, and it can be used to identify the location and strength of vortices over time. This information is valuable for understanding fluid flow behavior and designing fluid flow systems for specific applications. In this study, the Q criteria was applied to calculate the presence of vortices in a wind farm. When the Q criteria value is high, it indicates that vortices are capturing the uniform flow and reducing the performance of the wind turbine. Vortex flow can also increase the separated flow over the leading edge and increase drag forces. Therefore, understanding the behavior of vortices in fluid flow is essential for optimizing the performance of wind turbines and other fluid flow systems. The present study utilizes Q criteria, which incorporates the analysis of turbulence fields and detects the higher performance of rows in wind turbine farms to provide a better analysis in fluid physical concepts. This approach is motivated by the need to use novel criteria for calculating the weak points of wind turbines and to optimize the application of the corona actuator for high performance (Ekonomou et al., 2012; Blaabjerg et al., 2006; Liu et al., 2021; Hodgson et al., 2022; Oehme et al., 2022; Chen et al. 2023).

3.2 Validation of Results

The purpose of this section is to validate the current numerical results against the relevant experimental work.

Table 4 Mesh independent test

Number of Mesh	**Average Q criteria**
9×10^6	461.1
5×10^6	461.2
1×10^6	440.3
0.5×10^6	431.2

Table 5 Validation of results with the experimental study by Zheng et al. (2013) on the Ionic Charge Density of corona plasma

Length of electrodes	Ionic Charge Density (C/m^3)	
	Present Work	Zheng et al. (2013) work
2 cm	0.0015	0.0012
4 cm	0.0022	0.0021
6 cm	0.0037	0.0035
8 cm	0.0021	0.0020

Zheng et al. (2013) conducted an experiment to investigate the effect of using a plasma actuator on the flow over a flat and curved plate, aiming to apply the phenomenon of Corona plasma formation and discharge to a wind turbine. The study was used to validate the Corona discharge phenomenon. The study's specifications include an air density of 3 Kg/m^3, a peak-to-peak voltage of 20 kV, and a frequency of 14 Hz. The maximum error reported, calculated using the root mean square error formula, is 6%. Results were compared with the experimental study by Zheng et al. (2013), showcasing the Ionic Charge Density of corona plasma in Table 5. The differences observed in the far-field region can be attributed to the numerical method used to estimate the length of the plasma jet, its expansion length, maximum charge density, and numerical discretization methods for the fluid flow equations. However, the upgraded electrostatic model used to simulate the effect of the plasma actuator is accurate enough to continue the calculations. The second stage of validation involved comparing the experimental results of Fadaei et al. (2020) with the current numerical results of the pressure distribution around the airfoil at a 20° angle. Figure 3 was used to compare the pressure coefficient around the suction and pressure surfaces of the airfoil. The comparison revealed a maximum error of 2% using the root mean square error formula. The mesh-independent test indicated that 5×10^6 meshes are sufficient to ensure the independence of results from meshing, as shown in Table 4. Figures 3 illustrate the stagnation point and suction and pressure zones for the 2D airfoil of the wind turbine with and without the corona plasma actuator. The figures demonstrate that applying the corona plasma reduces the separation zone.

4. RESULTS

4.1. The Effect of Corona Discharge Frequency on Wind Turbine Farm Performance

The effects of adding a plasma actuator to a wind turbine blade depend on various parameters such as the

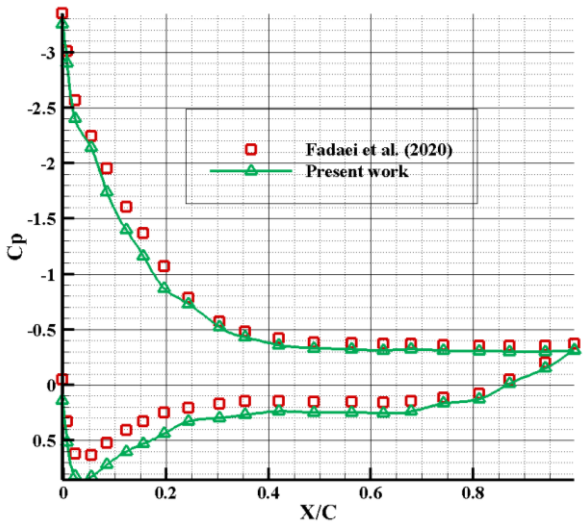

Fig. 3 Validation of results with the experimental study conducted by Fadaei et al. (2020) for pressure coefficient distribution with corona plasma

distance between the electrodes, thickness of dielectric layers, voltage level, frequency, and waveform shape. The effect of this actuator on aerodynamic parameters of the airfoil of the wind turbine blade under study, such as flow separation (vortex formation at the blade tip) and lift and drag coefficients for the two-dimensional case, was investigated. In this part of the study, the effect of the applied frequency to the electrodes on the flow characteristics around the airfoil at an angle of attack of 20° was examined. Table 6 shows the lift and drag coefficients, aerodynamic efficiency, and separation location at the tip of the wind turbine blade with and without the plasma discharge actuator at a voltage of 12 kV and various applied frequencies. It can be seen from Table 6 that as the applied frequency to the electrodes increases, the lift coefficient increases, and the drag coefficient decreases, resulting in an increase in the aerodynamic efficiency of the blade. Moreover, the flow separation point at the tip of the blade is delayed and moves further away from the angle of attack. This is because as the frequency increases, the length of the plasma jet and the volume force applied to the flow increases, which leads to an increase in the injected momentum into the near-wall flow, preventing rapid flow detachment. However, the width of the separated region decreases. The separation zone on a wind turbine blade is a distinct area where the air flow separates from the blade's surface. This results in a reduction in lift and an increase in drag, which could negatively impact the turbine's efficiency. Designers can use various strategies, such as airfoil shaping and blade twist, to mitigate separation zones and improve performance. The extent of the separation zone can be measured and monitored using X_{sep} measurements in tables, which provide information about the starting points of the separation and enable improvements in turbine performance to be tracked. Specifically, X_{sep} is considered to be zero for the primary case without plasma corona, and by adding plasma corona, this value (X_{sep}) shifts to the leading edges of the wind turbine.

Table 6 Effects of corona discharge frequency on performance criterions in wind turbine farm

(kHz) Frequency	X_{sep}	C_D	C_L
0	0.000 m	0.200	0.540
3	0.045 m	0.101	0.690
8	0.062 m	0.098	0.840
13	0.070 m	0.120	0.750

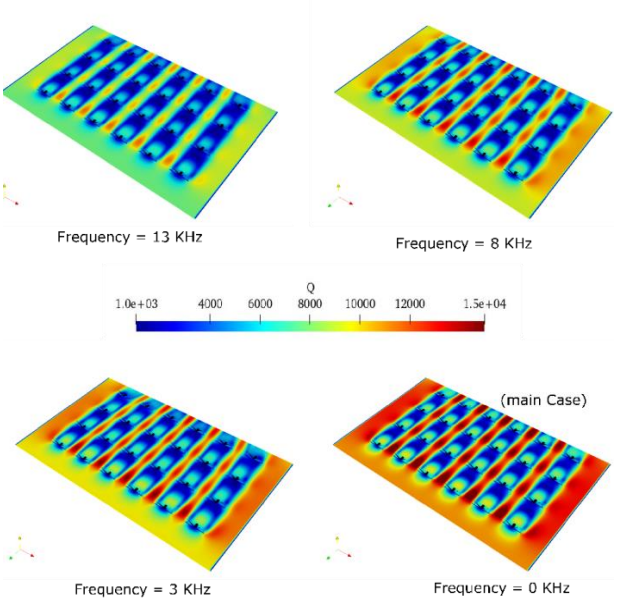

Fig. 4 Contours of effects of corona discharge frequency on Q criteria in wind turbine farm

4.2 The Effect of Corona Discharge Voltage on Wind Turbine Farm Performance

Considering that the applied voltage to the plasma field causes corona current excitation, this part of the study investigates the effect of applied voltage to the electrodes on the flow characteristics around the wind turbine blade at angle of attack of 20 °. Changes in lift coefficient, drag coefficient, and aerodynamic efficiency are presented in Table 7. Additionally, Fig. 5 show the Q contour diagram for voltages of 17, 12 and 7, respectively. It can be observed from the diagram that the positive effect of the applied plasma actuator on the mentioned parameters increases with increasing voltage. It can be seen that at a voltage of 12 kV, the effect of voltage is more pronounced in delaying the flow separation. This is due to the equations governing the plasma discharge modeling and the stronger effect of voltage compared to frequency on the length of the plasma jet and the induced trust due to the applied volume force. The voltage used in plasma corona discharge is a critical factor that affects the efficiency of the technology. The voltage must be high enough to ionize the air molecules but not so high as to cause a breakdown of the air molecules. The voltage required for plasma corona discharge to be effective in wind turbines varies depending on the specific design of the wind turbine and the operating conditions. Several studies have investigated the effect of the voltage of plasma corona discharge on the reduction of the separation

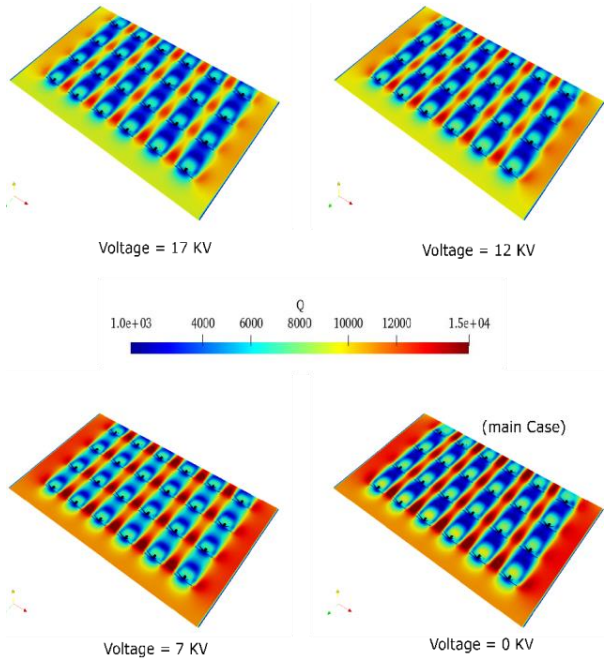

Fig. 5 Contours of effects of corona discharge voltage on Q criteria in wind turbine farm

Table 7 Effects of corona discharge Voltage on performance criterions in wind turbine farm

(KV) Voltage	X_{sep}	C_D	C_L
0	0.000 m	0.200	0.540
7	0.070 m	0.140	0.650
12	0.073 m	0.140	0.920
17	0.080 m	0.147	0.990

zone in wind turbines. These studies have shown that an increase in voltage can lead to a decrease in the separation zone and an increase in the power output of the wind turbine. However, there is a limit to the voltage that can be applied before the air molecules break down and the efficiency of the technology is reduced. Furthermore, the voltage of plasma corona discharge can affect the ion density and distribution of the plasma, which in turn affects the reduction of the separation zone. Higher voltages can lead to a higher ion density and a more uniform distribution of the plasma, resulting in a more efficient reduction of the separation zone.

4.3 The Effect of Distance Between Electrodes in Corona Discharge on Wind Turbine Farm Performance

Present part of research investigates the important parameters effect on plasma corona discharge performance located in the leading edge of wind turbine farms. The performance of corona discharge in wind turbines is influenced by several factors, including the distance between the electrodes. The distance between the electrodes determines the strength of the electric field and the intensity of the corona discharge. If the distance between the electrodes is too small, the electric field may be too strong, leading to a breakdown of the air molecules and a loss of efficiency. On the other hand, if the distance between the electrodes is too large, the electric field may not be strong enough to ionize the air molecules, leading to little or no effect on the separation zone. Therefore, finding the optimal distance between the electrodes is essential for maximizing the performance of corona discharge in wind turbines. This distance can vary depending on the specific design of the wind turbine and the operating conditions, and it may require some experimentation to determine the ideal distance. The optimal distance must be determined for each specific application to achieve the best performance. By optimizing the distance between the electrodes, wind turbine efficiency can be improved, leading to a more sustainable and cost-effective source of energy. In this study, three different distances between electrodes (3, 4, and 5 mm) were investigated to determine their effect on wind turbine performance. The results indicated that an increase in electrode distance resulted in a decrease in the distribution of the Q criteria. Essentially, this means that a larger electrode distance leads to a reduction in wind turbine performance. When the Q criteria is high, it indicates that the wake flow is dominating the active fluid flow type and decreasing the lift force of the wind turbine. Table 8 presents the impact of the distance between electrodes of corona discharge on performance criteria such as drag and lift forces, as well as the separation points of flow from the attack point in wind turbine farms.

Table 8 Effects of distance between electrodes of corona discharge on performance criteria in wind turbine farm

Distance between electrodes (mm)	X_{sep}	C_D	C_L
0	0.000 m	0.200	0.540
3	0.060 m	0.123	0.640
4	0.055 m	0.140	0.750
5	0.052 m	0.148	0.810

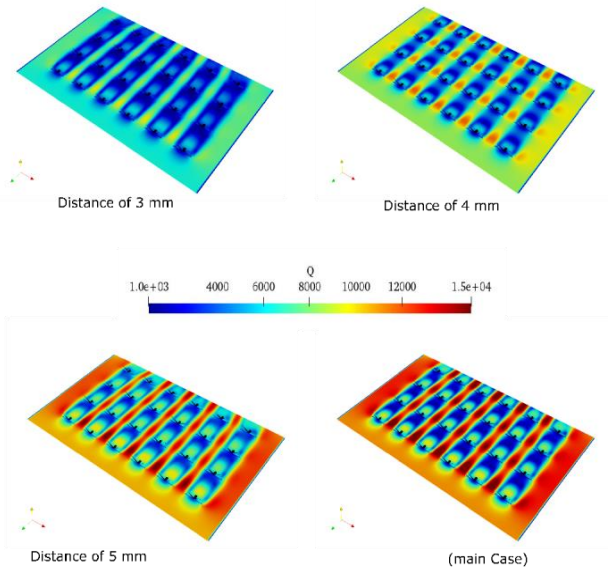

Fig. 6 Contours of effects of distance between electrodes of corona discharge on Q criteria in wind turbine farm

Table 9 Effects of corona discharge on performance of wind turbine farm produced power

Designed wind turbine farm	Wind turbine Power
Distance between electrodes of 3 mm, Voltage of 17 KV, and Frequency of 13 kHz	2.076 MW
Without corona plasma	2 MW

4.4. The Effect of Corona Discharge on Wind Turbine Farm Produced Power

Wind turbine farms are becoming increasingly popular as a renewable energy source and their power generation is influenced by several factors including wind speed, air density, blade length, and coefficient of performance (Cp). The formula used to calculate the power output of a wind turbine is $P = 0.5\ Cp\ \rho\pi R^2V^3$. Cp measures the efficiency of the turbine and reflects the proportion of wind energy that can be converted into electrical power. Air density affects the amount of energy that can be extracted from the wind, while blade length and wind speed are critical factors in determining power output. Betz's law limits the maximum amount of power that can be extracted to 59.3% of the wind's kinetic energy, making 59.3% the maximum possible turbine efficiency. The plasma corona discharge technology has been shown to improve the aerodynamics of wind turbine blades and increase power production by reducing drag, turbulence, and increasing lift force and rotational speed. Additionally, the technology can reduce the frequency of blade cleaning and maintenance. One of the key advantages of plasma corona discharge technology is that it can be installed on existing wind turbines without significant modifications. Table 9 compares two case studies, one with plasma corona discharge and the other without. The wind turbine farm with plasma corona discharge on the leading edge of the blades showed a significant increase in power production compared to the farm without the technology. The difference in power output suggests that plasma corona discharge technology has a positive impact on the power production of wind turbine farms. In summary, the power produced by wind turbines depends on several factors, and the plasma corona discharge technology has the potential to improve efficiency and performance, making it a valuable technology for wind turbine farms.

In order to enhance the analysis of wind turbine farms, we took measurements of spanwise velocity, pressure, epsilon, and turbulent kinetic energy. A high spanwise velocity has the potential to reduce power output due to the opposite direction of the rotating flow. This concept is further elaborated in the work of Ramesh Kumar and Selvaraj (2023b). High spanwise velocity signifies a negative flow direction, which leads to an increase in drag force and has a negative effect on power output. The pressure distribution on the first row of wind turbines is higher than that of other rows, as the first row is exposed to uniform flow and the wake flow has a significant effect on its performance. Figure 7 shows two essential parameters related to the turbulent model, kinematic and epsilon contours. The results indicate that epsilon dissipation is higher at middle rows of the wind turbine

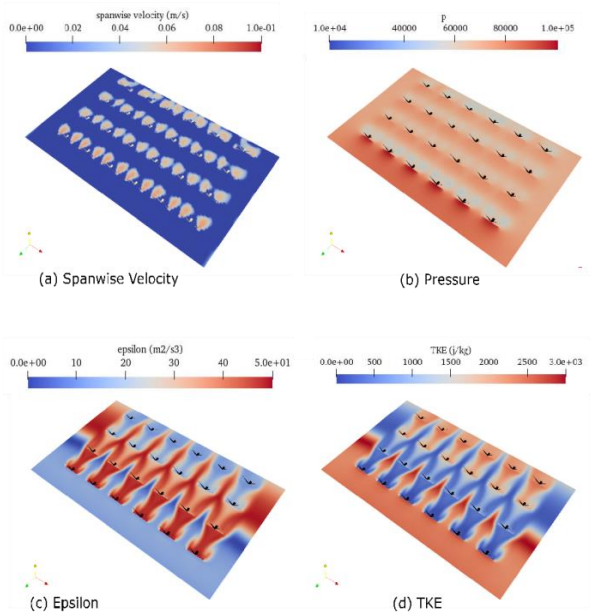

Fig. 7 Contours of (a) spanwise velocity, (b) pressure, (c) epsilon, and (d) turbulent kinetic energy in wind turbine farm

farm. Additionally, the first rows are highly influenced by kinematic turbulence energy due to high velocity distributions. Higher kinematic turbulence and epsilon in wind farms refer to an increase in turbulence and the dissipation of energy within the rotating flow of the wind turbines. Kinematic turbulence represents the energy associated with the turbulent motion of the wind flow. A higher kinematic turbulence indicates that the wind flow has a higher velocity distribution and is more turbulent, which can affect the performance of the wind turbine blades. Epsilon, on the other hand, measures the rate at which kinetic energy is converted into heat due to turbulent motion. A higher epsilon indicates more energy dissipation within the rotating flow of the wind turbines, which can impact the performance of the turbine blades by influencing the lift and drag forces acting on them. Thus, higher kinematic turbulence and epsilon can have a negative impact on the power output of a wind farm by increasing drag force and decreasing lift force on the turbine blades.

5. CONCLUSION

The aim of this research was to use the *OPENFOAM* software to conduct numerical simulations and compare the results obtained with and without the plasma actuator at an angle of attack of 20 °. The study found that while the plasma actuator induced momentum and accelerated flow towards the suction side, the flow resisted against the pressure gradient unfavorably. However, the flow eventually recovered to an appropriate pressure, and this pressure recovery improved with an increase in the plasma actuator voltage. An increase in frequency also led to improved pressure recovery, and the research demonstrated delayed flow separation with increasing frequency and voltage. The results showed that using a

corona discharge-based plasma actuator can increase the efficiency of wind turbine farms and enhance the aerodynamic coefficients. The study also found that increasing the voltage and frequency of the corona discharge, as well as decreasing the distance between electrodes, can reduce the Q criteria. Additionally, the study examined the effects of pressure, turbulent kinetic energy, spanwise velocity, and epsilon on power generation in a wind turbine farm. The results are summarized below.

- Introducing corona plasma at the leading edge of wind turbine blades increased power production by more than 3.8%.

- The corona plasma actuator utilized electrodes spaced 3 mm apart, with a voltage of 17 KV and a frequency of 13 kHz.

- The study recommends future experimental validation of the findings and consideration of real-world factors such as relative humidity and wind flow direction.

- Strong support is expressed in the study for the implementation of corona plasma actuators on wind turbines to enhance power production.

ACKNOWLEDGEMENTS

Authors want to thank faculty members of Kish International Campus in University of Tehran.

CONFLICT OF INTEREST

There is no conflict of interest.

AUTHORS CONTRIBUTION

S. Abed: Methodology, Software, Data curation, Writing original draft, Validation. **S. Karimian:** Review and Editing, Validation, Project Administration. **S. K. Ghaemi Osgouei:** Methodology, Review and Editing, Software, Supervision. **M. Moshfeghi:** Data curation, Validation, Conceptualization, Writing original draft.

REFERENCES

Abdolahipour, S., Mani, M., & Shams Taleghani, A. (2022). Pressure improvement on a supercritical high-lift wing using simple and modulated pulse jet vortex generator. *Flow, Turbulence and Combustion, 109*(1), 65-100. https://doi.org/10.1007/s10494-022-00327-9

Abdolahipour, S., Mani, M., & Taleghani, A. S. (2021). Parametric study of a frequency-modulated pulse jet by measurements of flow characteristics. *Physica Scripta, 96*(12), 125012. https://doi.org/10.1088/1402-4896/ac2bdf

Abdollahzadeh, M., Pascoa, J. C., & Oliveira, P. J. (2014a). Modified split-potential model for modeling the effect of DBD plasma actuators in high altitude flow control. *Current Applied Physics, 8*(14), 1160-1170. https://doi.org/10.1016/j.cap.2014.05.016

Abdollahzadeh, M., Páscoa, J. C., & Oliveira, P. J. (2014b). Two-dimensional numerical modeling of interaction of micro-shock wave generated by nanosecond plasma actuators and transonic flow. *Journal of Computational and Applied Mathematics, 270*, 401-416. https://doi.org/10.1016/j.cam.2013.12.030

Abdollahzadeh, M., Pascoa, J. C., & Oliveira, P. J. (2018). Comparison of DBD plasma actuators flow control authority in different modes of actuation. *Aerospace Science and Technology, 78*, 183-196. https://doi.org/10.1016/j.ast.2018.04.013

Abed ZahmatkeshPasand, S., Ghaemi Osgouie, S. K., Karimian Aliabadi, S., & Moshfeghi, M. (2023). Numerical study of the effect of weather parameters on corona discharge performance in a horizontal axis wind turbine. International *Journal of Nonlinear Analysis and Applications*, *14*(12), 187-196 https://doi.org/10.22075/ijnaa.2022.29450.4170

Belabes, B., & Paraschivoiu, M. (2023). CFD modeling of vertical-axis wind turbine wake interaction. *Transactions of the Canadian Society for Mechanical Engineering*, 47, 449-458 https://doi.org/10.1139/tcsme-2022-0149

Benard, N., & Moreau, E. (2014). Electrical and mechanical characteristics of surface AC dielectric barrier discharge plasma actuators applied to airflow control. *Experiments in Fluids*, *11*(55), 1-43. https://doi.org/10.1007/s00348-014-1846-x

Benmoussa, A., & Páscoa, J. C. (2023). Enhancement of a cycloidal self-pitch vertical axis wind turbine performance through DBD plasma actuators at low tip speed ratio. *International Journal of Thermo-fluids, 17*, 100258. https://doi.org/10.1016/j.ijft.2022.100258

Blaabjerg, F., Chen, Z., Teodorescu, R., & Iov, F. (2006). *Power electronics in wind turbine systems.* 2006 CES/IEEE 5th International Power Electronics and Motion Control Conference (Vol. 1, pp. 1-11). IEEE. https://doi.org/10.1109/IPEMC.2006.4777946

Chen, C., Wang, L., & Niu, M. (2023). Research on the application of improved NSGA-II in the structure design of wind turbine blade spar cap. *Frontiers in Energy Research, 11*, 1160423. https://doi.org/10.3389/fenrg.2023.1160423

De Giorgi, M. G., Motta, V., Suma, A., & Lafori, A. (2021). Comparison of different plasma actuation strategies for aeroelastic control on a linear compressor cascade. *Aerospace Science and Technology, 117*, 106902. https://doi.org/10.1016/j.dib.2021.107584

Durscher, R., & Roy, S. (2012). Evaluation of thrust measurement techniques for dielectric barrier discharge actuators. *Experiments in Fluids, 4*(53), 1165-1176. https://doi.org/10.1007/s00348-012-1349-6

Ebrahimi, A., & Hajipour, M. (2018). Flow separation control over an airfoil using dual excitation of DBD plasma actuators. *Aerospace Science and Technology*, *79*, 658-668. https://doi.org/10.1016/j.ast.2018.06.019

Ebrahimi, A., Hajipour, M., & Ghamkhar, K. (2018). Experimental study of stall control over an airfoil with dual excitation of separated shear layers. *Aerospace Science and Technology*, *82*, 402-411. https://doi.org/10.1016/j.ast.2018.09.027

Ekonomou, L., Lazarou, S., Chatzarakis, G. E., & Vita, V. (2012). Estimation of wind turbines optimal number and produced power in a wind farm using an artificial neural network model. *Simulation Modelling Practice and Theory*, *21*(1), 21-25. https://doi.org/10.1016/j.simpat.2011.09.009

El Kasmi, A., & Masson, C. (2008). An extended k–ε model for turbulent flow through horizontal-axis wind turbines. *Journal of Wind Engineering and Industrial Aerodynamics*, *96*(1), 103-122. https://doi.org/10.1016/j.jweia.2007.03.007

Enloe, C. L., McLaughlin, T. E., VanDyken, R. D., Kachner, K. D., Jumper, E. J., & Corke, T. C. (2004). Mechanisms and responses of a single dielectric barrier plasma actuator: plasma morphology. *AIAA Journal*, *3*(42), 589-594. https://doi.org/10.2514/1.3884

Fadaei, M., Davari, A., Sabetghadam, F., & Soltani, M. R. (2020). Investigation of single dielectric barrier discharge plasma actuator effect on separation control of a critical section of wind turbine blade. *Modares Mechanical Engineering*, *9*(20), 2289-2302. http://dorl.net/dor/20.1001.1.10275940.1399.20.9.4.1

Guerra‐Garcia, C., Nguyen, N. C., Mouratidis, T., & Martinez‐Sanchez, M. (2020). Corona discharge in wind for electrically isolated electrodes. *Journal of Geophysical Research: Atmospheres*, *125*(16), e2020JD032908. https://doi.org/10.1029/2020JD032908

Gulski, E., Anders, G. J., Jongen, R. A., Parciak, J., Siemiński, J., Piesowicz, E., & Irska, I. (2021). Discussion of electrical and thermal aspects of offshore wind farms' power cables reliability. *Renewable and Sustainable Energy Reviews*, *151*, 111580. https://doi.org/10.1016/j.rser.2021.111580

Hodgson, E. L., Grinderslev, C., Meyer Forsting, A. R., Troldborg, N., Sørensen, N. N., Sørensen, J. N., & Andersen, S. J. (2022). Validation of aeroelastic actuator line for wind turbine modelling in complex flows. *Frontiers in Energy Research*, *10*, 864645. https://doi.org/10.3389/fenrg.2022.864645

Ibrahim, I. H., & Skote, M. (2011). Boundary condition modifications of the suzen-huang plasma actuator model. *International Journal of Flow Control*, *3*. https://doi.org/10.1260/1756-8250.3.2-3.111

Kaviani, H. R., & Moshfeghi, M. (2023). Multi-megawatt horizontal axis wind turbine blade optimization based on PSO method. *Aerospace*, *10*(2), 158. https://doi.org/10.3390/aerospace10020158

Liu, Y., Liu, S., Zhang, L., Cao, F., & Wang, L. (2021). Optimization of the yaw control error of wind turbine. *Frontiers in Energy Research*, *9*, 626681. https://doi.org/10.3389/fenrg.2021.626681

Maas, O. (2023). Large-eddy simulation of a 15 GW wind farm: Flow effects, energy budgets and comparison with wake models. *Frontiers in Mechanical Engineering*, *9*, 1108180. https://doi.org/10.3389/fmech.2023.1108180

Mirzaei, M., Taleghani, A. S., & Shadaram, A. (2012). Experimental study of vortex shedding control using plasma actuator. *Applied Mechanics and Materials*, *186*, 75-86. https://doi.org/10.4028/www.scientific.net/AMM.186.75

Mohammadi, M., & Taleghani, A. S. (2014). Active flow control by dielectric barrier discharge to increase stall angle of a NACA0012 airfoil. *Arabian Journal for Science and Engineering*, *39*, 2363-2370. https://doi.org/10.1007/s13369-013-0772-1

Nazari, A., Jafari, M., Rezaei, N., Taghizadeh-Hesary, F., & Taghizadeh-Hesary, F. (2021). Jet fans in the underground car parking areas and virus transmission. *Physics of fluids*, *33*(1), 013603. https://doi.org/10.1063/5.0033557

Nazari, A., Wang, C., He, R., Taghizadeh-Hesary, F., & Hong, J. (2023). Numerical investigation of airborne infection risk in an elevator cabin under different ventilation designs. *Physics of Fluids*, *35*(6). https://doi.org/10.1063/5.0152878

Oehme, F., Gleichauf, D., Balaresque, N., Sorg, M., & Fischer, A. (2022). Thermographic detection and localization of unsteady flow separation on rotor blades of wind turbines. *Frontiers in Energy Research*, *10*, 1043065. https://doi.org/10.3389/fenrg.2022.1043065

Omidi, J., & Mazaheri, K. (2017). Improving the performance of a numerical model to simulate the EHD interaction effect induced by dielectric barrier discharge. *International Journal of Heat and Fluid Flow*, *67*(5), 79-94. http://dx.doi.org/10.1016/j.ijheatfluidflow.2017.07.008

Qu, J., Zeng, M., Zhang, D., Yang, D., Wu, X., Ren, Q., & Zhang, J. (2021). A review on recent advances and challenges of ionic wind produced by corona discharges with practical applications. *Journal of Physics D: Applied Physics*, *55*(15), 153002. https://doi.org/10.1088/1361-6463/ac3e2c

Qu, L., Wang, Y., Liu, G., Liao, M., Cai, H., Zhang, T., Deng, Y. & Wen, X. (2019). Simulation study on positive corona discharge of receptors on rotating wind turbine blade tips under thundercloud electric fields. *Energies*, *12*(24), 4696.

https://doi.org/10.3390/en12244696

Ramesh Kumar, K., & Selvaraj, M. (2023a). Investigations on integrated funnel, fan and diffuser augmented unique wind turbine to enhance the wind speed. *Journal of Applied Fluid Mechanics, 16*(3), 575-589. https://www.jafmonline.net/article_2166.html

Ramesh Kumar, K., & Selvaraj, M. (2023b). Novel deep learning model for predicting wind velocity and power estimation in advanced INVELOX wind turbines. *Journal of Applied Fluid Mechanics, 16*(6), 1256-1268. https://www.jafmonline.net/article_2221.html

Roth, J. R. (2003). Aerodynamic flow acceleration using paraelectric and peristaltic electrohydrodynamic effects of a one atmosphere uniform glow discharge plasma. *Physics of Plasmas, 5*(10), 2117-2126. https://doi.org/10.1063/1.1564823

Salmasi, A., Shadaram, A., & Taleghani, A. S. (2013). Effect of plasma actuator placement on the airfoil efficiency at post stall angles of attack. *IEEE Transactions on Plasma Science, 41*(10), 3079-3085. https://doi.org/10.1109/TPS.2013.2280612

Sanderse, B., Van der Pijl, S. P., & Koren, B. (2011). Review of computational fluid dynamics for wind turbine wake aerodynamics. *Wind energy, 14*(7), 799-819. https://doi.org/10.1002/we.458

Shams Taleghani, A., Shadaram, A., Mirzaei, M., & Abdolahipour, S. (2018). Parametric study of a plasma actuator at unsteady actuation by measurements of the induced flow velocity for flow control. *Journal of the Brazilian Society of Mechanical Sciences and Engineering, 40*, 1-13. https://doi.org/10.1007/s40430-018-1120-x

Shams Taleghani. A., Shadaram, A., & Mirzaei, M. (2012). Effects of duty cycles of the plasma actuators on improvement of pressure distribution above a NLF0414 airfoil. *IEEE Transactions on Plasma Science, 40*(5), 1434-1440. https://doi.org/10.1109/TPS.2012.2187683

Sheikholeslam Noori, S. M., Shams Taleghani, S. A., & Taeibi, M. (2020a). Phenomenological investigation of drop manipulation using surface acoustic waves. *Microgravity Science and Technology, 32*, 1147-1158. https://doi.org/10.1007/s12217-020-09839-3

Sheikholeslam Noori, S. M., Shams Taleghani, S. A., & Taeibi, M. (2021). Surface acoustic waves as control actuator for drop removal from solid surface. *Fluid Dynamics Research, 53*(4), 045503. https://doi.org/10.1088/1873-7005/ac12af

Sheikholeslam Noori, S. M., Taeibi, M., & Shams Taleghani, S. A. (2020b). Effects of contact angle hysteresis on drop manipulation using surface acoustic waves. *Theoretical and Computational Fluid Dynamics, 34*, 145-162. https://doi.org/10.1007/s00162-020-00516-0

Sheikholeslam Noori, S. M., Taeibi, M., & Shams Taleghani, S. A. (2020c). Numerical analyses of droplet motion over a flat plate due to surface acoustic waves. *Microgravity Science and Technology, 32*, 647-660. https://doi.org/10.1007/s12217-020-09784-1

Sinner, M., Petrović, V., Stockhouse, D., Langidis, A., Pusch, M., Kühn, M., & Pao, L. Y. (2023). Insensitivity to propagation timing in a preview-enabled wind turbine control experiment. *Frontiers in Mechanical Engineering, 9*, 1145305. https://doi.org/10.3389/fmech.2023.1145305

Suzen, Y. B., & Huang, P. G. (2005). Numerical simulation of unsteady wake/blade interactions in low-pressure turbine flows using an intermittency transport equation, *Journal of Turbomachinery, 127*(3), 431-444. 431-444. https://doi.org/10.1115/1.1860375

Taeibi, M., Shams Taleghani, S. A., Sheikholeslam Noori, S. M., & Ahmadi, G. (2022). Computational simulation of water removal from a flat plate, using surface acoustic waves. *Wave Motion, 111*, 102867. https://doi.org/10.1016/j.wavemoti.2021.102867

Thomas, F. O., Corke, T. C., Iqbal, M., Kozlov, A., & Schatzman, D. (2009). Optimization of dielectric barrier discharge plasma actuators for active aerodynamic flow control. *AIAA Journal, 9*(47), 2169-2178. https://doi.org/10.2514/1.41588

Wang, J., Cai, Y. X., Li, X. H., Shi, Y. F., Bao, Y. C., Wang, J., & Shi, Y. X. (2018). Ionic wind development in corona discharge for LED cooling. *IEEE Transactions on Plasma Science, 46*(5), 1821-1830. https://doi.org/10.1109/TPS.2018.2816820

Yang, J., & Zhang, W. (2023). Forced response analysis of the rotor blade rows with the ROM-based aeroelastic model. *Aerospace Science and Technology, 139*, 108366. https://doi.org/10.1016/j.ast.2023.108366

Yu, W., Li, Q., Zhao, J., & Siew, W. H. (2022). Numerical simulation of the lightning leader development and upward leader initiation for rotating wind turbine. *Machines, 10*(2), 115. https://doi.org/10.3390/machines10020115

Zhang, Y. N., Wang, X. Y., Zhang, Y. N., & Liu, C. (2019). Comparisons and analyses of vortex identification between Omega method and Q criterion. *Journal of Hydrodynamics, 31*, 224-230. https://doi.org/10.1007/s42241-019-0025-1

Zheng, Y., Hu, C., Sheng, P., & Zhang, X. (2013). Design of timing synchronization software on EAST-NBI. *Plasma Science and Technology, 15*(12), 1237. https://doi.org/10.1088/1009-0630/15/12/14